Growth of Self-Organized Hierarchical ZnO Nanoarchitectures by a Simple In/In_2S_3 Controlled Thermal Evaporation Process

Guozhen Shen,*,†,‡ Yoshio Bando,† and Cheol-Jin Lee*,‡

Advanced Materials Laboratory, National Institute for Materials Science, Namiki 1-1, Tsukuba, Ibaraki 305-0044, Japan, and Department of Nanotechnology, Hanyang University, 17-Haengdang-dong, Seongdong-gu, Seoul 133-791, South Korea

Received: February 24, 2005; In Final Form: April 5, 2005

Novel hierarchical ZnO nanoarchitectures, such as microtrepangs, microbelts, nanoflowers, nanocombs, nanowheels, and nanofans assembled by ZnO nanocones, nanobowling pins, nanobottles, nanoarrows, and nanonails, have had their growth controlled by the thermal evaporation of Zn and a mixture of In and In_2S_3. Both the morphologies of the products and their construction units could be efficiently controlled by simple adjustment of the weight ratio of In/In_2S_3. The phase structure, morphologies, and photoluminescence properties of the ZnO products were investigated by X-ray diffraction, scanning electron microscopy, high-resolution transmission electron microscopy, and photoluminescence spectroscopy. These novel hierarchical ZnO nanoarchitectures may be attractive building blocks for creating optical or other nanodevices.

1. Introduction

One-dimensional nanostructures, such as nanowires, nanotubes, and nanobelts, have stimulated intensive interest in recent years due to their unique properties in mesoscopic physics and their applications to nanoscale devices based on their special properties compared with those of the corresponding bulk crystals.[1−7] As an important II−VI semiconductor, zinc oxide (ZnO) is of considerable interest due to its distinguished performance in electronics, optics, mechanics, and photonics. ZnO with a band gap of 3.37 eV and large exciton binding energy of 60 meV at room temperature is a key technological material.[8,9] The lack of a center of symmetry in wurtzite, combined with large electromechanical coupling, results in strong piezoelectric and pyroelectric properties and the consequent use of ZnO in mechanical actuators and piezoelectric sensors. A number of methods have been developed to synthesize ZnO one-dimensional nanostructures, such as nanowires, nanorods, nanobelts, and nanotubes using vapor-phase transport, thermal evaporation, simple gas reaction, template-directed wet and dry methods, and wet chemical routes.[4−23]

Many recent efforts on ZnO nanostructures have focused on the integration of one-dimensional ZnO nanoscale building blocks into two- and three-dimensional ordered superstructures or complex functional architectures, which is a crucial step toward the realization of functional nanosystems. For example, well-aligned ZnO nanowire arrays have been fabricated by several different methods including template methods, vapor transport and condensation methods, metal vapor deposition methods, and metal−organic source vapor deposition.[8,16,24−26] ZnO nanocombs,[15,27] ZnO nanopropellers,[28] and nanocantilever arrays[29] were also synthesized by a vapor transport and condensation technique. Moreover, novel self-organized nanobridges, nanonails, and other hierarchical nanostructures with different symmetries were obtained by the vapor-phase process.[30,31] These novel architectures indicate that ZnO contains probably the richest family of nanostructures among all materials, in both structures and properties. To obtain these novel nanostructures, ZnO is the general source material, usually high temperatures or very low pressures are required to decompose ZnO, and it still remains a significant challenge to develop facile, mild, and effective methods for creating hierarchical architectures assembled from one-dimensional ZnO nanostructures.

In this paper, we report the controlled growth of novel hierarchical nanoarchitectures, such as microtrepangs of ZnO nanocones, microbelts of ZnO nanobowling-pin arrays, nanoflowers of ZnO nanobottles, nanocombs and nanowheels of ZnO nanonarrows, and nanofans of ZnO nanonails using a simple atmospheric pressure thermal vapor deposition method. In this process, metallic zinc was used as the zinc source since the Zn vapor pressure can reach up to 10.8 Pa at a temperature down to 400 °C. In the process, both the morphology and the construction units can be efficiently controlled by a simple adjustment of the weight ratio of In/In_2S_3. Room-temperature photoluminescence studies of these nanoarchitectures show greatly enhanced green emission, which is of great interest for typical applications of ZnO phosphors.

2. Experimental Section

Material Synthesis. The hierarchical ZnO nanostructures were grown by the atmospheric pressure thermal evaporation of Zn powder and the mixture of In and In_2S_3 powders in a two-heating-zone furnace system. A p-type Si wafer was used as the substrate for deposition. Before the substrate was loaded into the furnace, it was ultrasonically cleaned in ethanol for 5 min and then rinsed with distilled water. In a typical procedure, Zn powder and the mixture of In and In_2S_3 powders with a controlled weight ratio were put into two ceramic boats separately in the two-heating-zone furnace. The mixture of In and In_2S_3 powders was put in the first heating zone (upstream), and the Zn powder was put in the second heating zone (downstream). And the substrate was placed downstream to

* Author to whom correspondence should be addressed. E-mail: gzshen@ustc.edu; cjlee@hanyang.ac.kr.
† National Institute for Materials Science.
‡ Hanyang University.

10.1021/jp050950c CCC: $30.25
Published on Web 04/29/2005

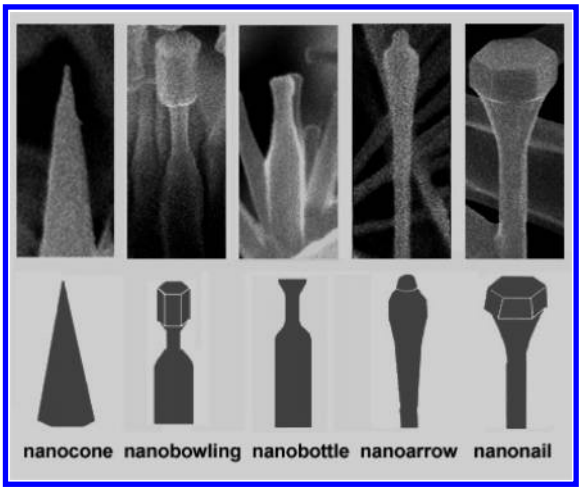

Figure 1. Schematic illustration of the construction units for different ZnO nanostructures.

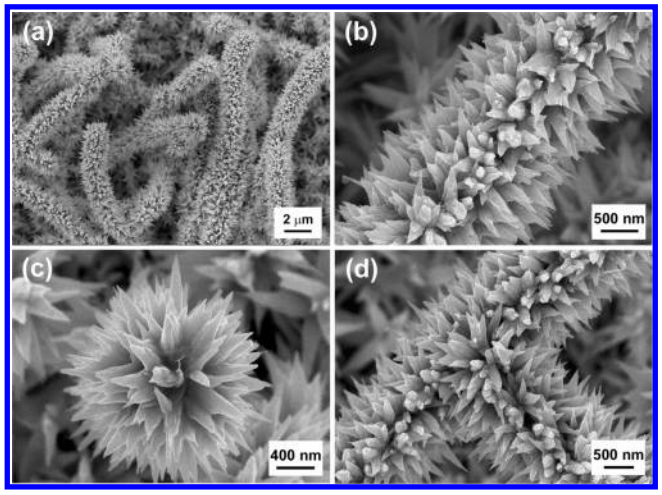

Figure 2. SEM images of the ZnO microtrepangs composed of ZnO nanocones: (a) low-magnification image, (b) side-view image, (c) top-view image, and (d) side view of a T-shaped microtrepang.

collect the products. The distance between the Zn powder and the Si substrate was set to 10 mm. The temperature of the Si substrate is about 500 °C in the system. The heating temperature of the Zn powder was set to 550 °C, and the heating temperature of the mixture of In and In_2S_3 was set to 900 °C. After the system was purged with high-purity Ar (99.999%) for 5−10 min, the system was heated to the desired temperature and kept at that temperature for 60 min with an Ar gas flow rate of 500 sccm. After being cooled to room temperature, the substrate was found to have been deposited with gray-white products.

Material Characterization. The morphologies were analyzed using scanning electron microscopy (SEM, Hitachi S-4700). The crystal structures of the products on substrates were characterized using X-ray diffraction (XRD, Rigaku D/Max-2500). The stoichiometric analysis of the products was performed by scanning electron microscopy equipped with energy dispersive X-ray (EDX) spectroscopy. And the microstructure analysis was conducted using high-resolution transmission electron microscopy (HRTEM, Tecnai F20). Photoluminescence (PL) measurements were performed at room temperature using a He−Cd laser line of 325 nm as an excitation source.

3. Results and Discussion

After thermal evaporation, several novel self-organized hierarchical nanoarchitectures were obtained. Studies found that

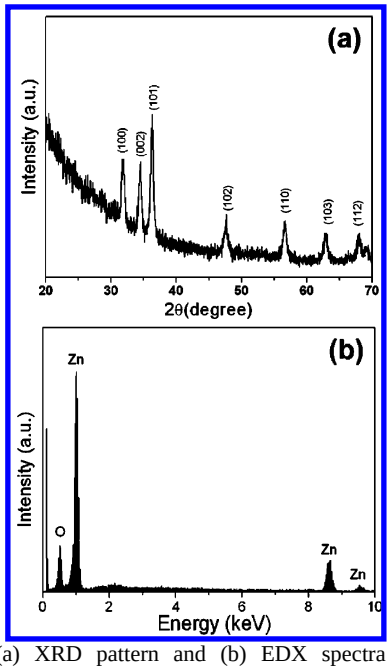

Figure 3. (a) XRD pattern and (b) EDX spectra of the ZnO microtrepang of nanocones.

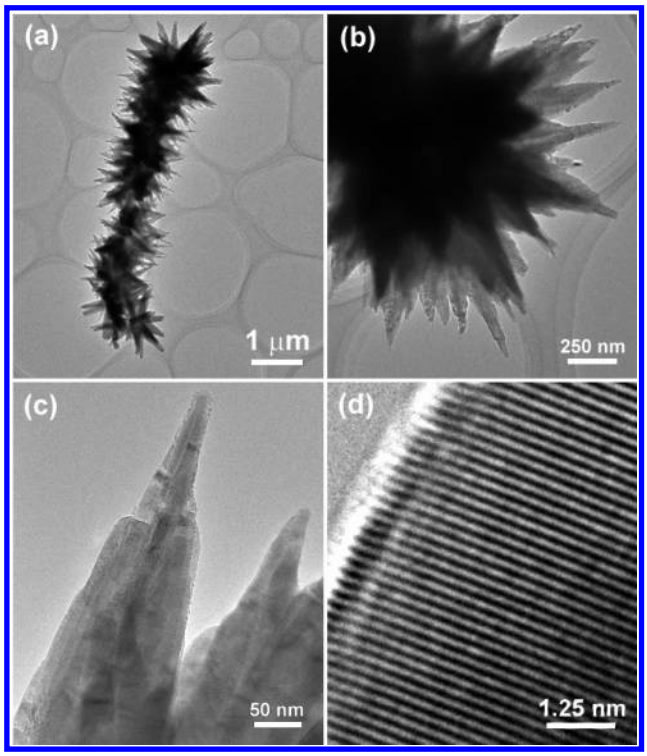

Figure 4. (a and b) TEM image of a single ZnO microtrepang, (c) TEM images of branched ZnO nanocones, (d) HRTEM image of an individual ZnO nanocone branch.

the construction units of these novel structures also varied greatly, including nanocones, nanobowling pins, nanobottles, nanoarrows, and nanonails.

Figure 1 shows schematic illustrations of these novel construction units as produced by our experiments. The synthesis and morphology of these construction units will be discussed in detail subsequently.

Microtrepangs of ZnO Nanocones. Figure 2 shows typical SEM images with different magnifications of the ZnO products obtained at an In/In_2S_3 weight ratio of 1:2. Large-scale novel trepanglike structures are obtained under the present experimental conditions. These novel trepanglike nanostructures have

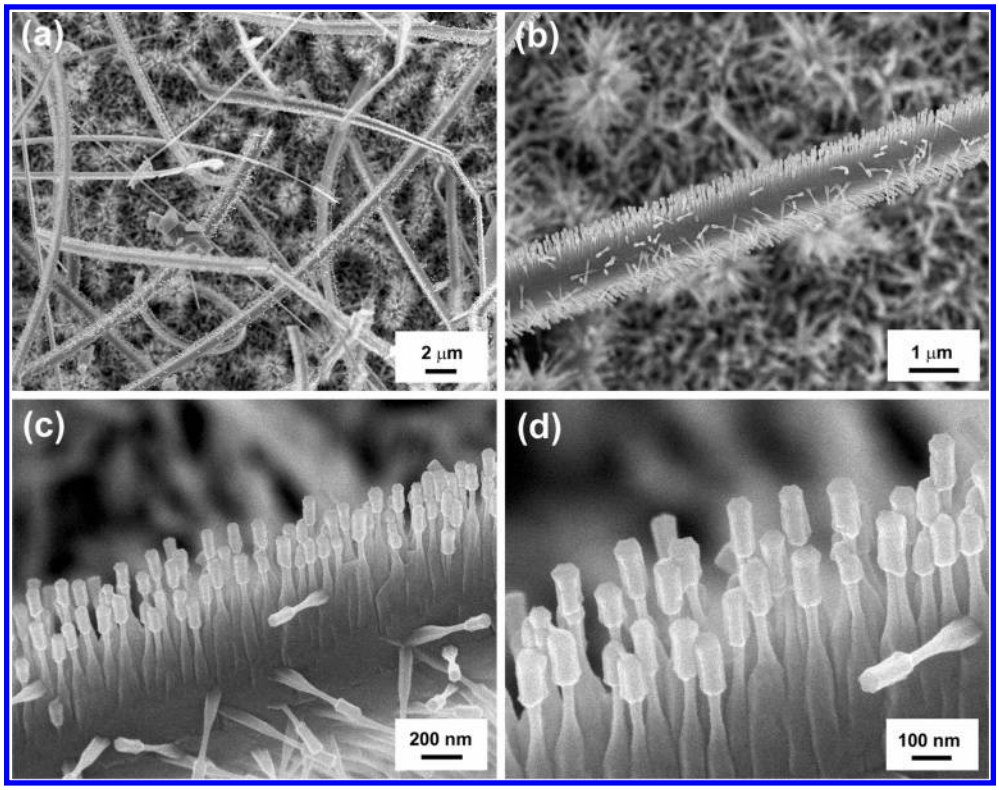

Figure 5. SEM images with different magnifications of microbelts of ZnO nanobowling-pin arrays when the weight ratio of In/In_2S_3 is 1:1.

lengths of 3−20 μm and uniform diameters of 1.5 μm as shown in Figure 2a. On each microtrepang, there are a number of uniform ZnO crystallites radially oriented along the main trunk. From the highly magnified SEM images shown in Figure 2b, it can be seen that each microtrepang is composed of high-density ZnO nanocones grown perpendicular along the main trunk. The lengths of the ZnO nanocones are about 200−500 nm, and the diameter of the microtrepang is about 1.5 μm. Figure 2c is the top view of a single ZnO microtrepang, which also confirms the assembly of ZnO nanocones to form microtrepangs. From the top-view image, many ZnO nanocones grow radially along the main trunk with special symmetry. We also find some T-shaped microtrepangs as shown in Figure 2d.

XRD was used to obtain the structure of the trepanglike ZnO nanostructures, and the pattern is shown in Figure 3a. All of the peaks in this pattern can be indexed to pure wurtzite ZnO with cell constants comparable to the reported values (Joint Committee on Powder Diffraction Standards (JCPDS) Card No. 36-1451). No peaks of other impurities such as Zn, In_2O_3, or ZnS were detected, indicating the relatively high purity of the ZnO products. EDX spectroscopy was used to obtain the compositions of the products. Figure 3b reveals that only Zn and O with an approximate atomic ratio of the Zn and O elements appear, which is comparable to the stoichiometric compound. The peak that appears at around 2 keV is that of gold, which comes from the SEM specimen preparation. By means of XRD and EDX analyses, no In was detected in the experimental error range. The results confirm the formation of the pure ZnO product instead of the doped ZnO.

The ZnO microtrepangs were further characterized using HRTEM. Figures 4a and 4b show the TEM images of a single ZnO microtrepang. They clearly indicate that there are many triangular ZnO nanocone branches grown perpendicular to the main trunk just as observed by SEM. Figure 4c is the TEM image of several branched nanocones grown on the main trunk. From the image, the needle-shaped tips of the cones can be clearly seen. The branched ZnO nanocone is of about 200−500 nm in length, consistent with the SEM results. The HRTEM image recorded from the edge of an individual side-branched ZnO nanocone shown in Figure 4d clearly shows the well-resolved interference lattice fringe of about 0.26 nm, which is consistent with the (002) parameter in the wurtzite ZnO phase, indicating that the branched ZnO nanocones grew preferentially along the [001] direction, which is the general growth direction for one-dimensional ZnO nanostructures. So our branched ZnO nanocones are single-crystalline, wurtzite-structured, and *c*-axis-elongated.

Microbelts of ZnO Nanobowling-Pin Arrays. When the weight ratio of In/In_2S_3 was increased to 1:1, another interesting hierarchical nanostructure, namely, microbelts of ZnO nanobowling-pin arrays, was obtained. Figure 5a shows the general morphology of the samples. Beltlike crystals with typical diameters of 1 μm and lengths up to tens of micrometers are deposited on the Si substrate. Figure 5b is a magnified SEM image of a single ZnO microbelt. Two sets of rodlike crystal arrays have perpendicular growth directions to the lengths of the microbelts. More interestingly, high-magnification SEM images, as shown in Figures 5c and 5d, reveal that the two sets of rodlike crystal arrays are actually of bowling-pin-like morphology, namely, ZnO nanobowling pins. Each nanobowling pin is composed of a hexagonal prism cap and a main trunk connected with a smaller diameter neck. The diameter of the hexagonal prism cap is 30 nm, and the typical height is 100 nm.

Nanoflowers of ZnO Nanobottles. Besides these novel microbelts of ZnO nanobowling-pin arrays, some flowerlike structures were also detected (Figure 5a). Careful adjustment of the weight ratio of In/In_2S_3 to 3:2 gave pure ZnO nanoflowers. Figure 6 shows the corresponding SEM images of ZnO nanoflowers. Large-scale ZnO nanoflowers are deposited on the whole Si substrate as shown in Figure 6a. Each nanoflower is about 2 μm in size with many petals radially grown from the

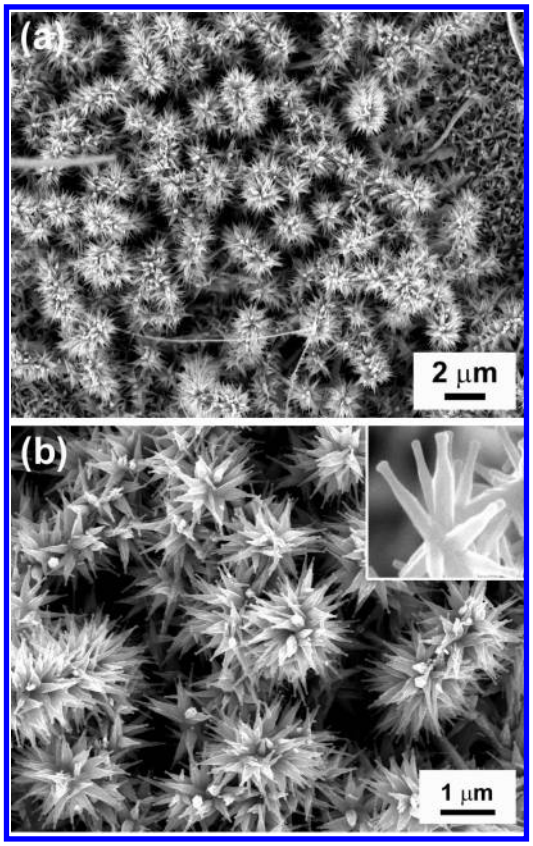

Figure 6. SEM images of nanoflowers of ZnO nanobottles when the weight ratio of In/In_2S_3 is 3:2.

center with spherical symmetry. Figure 6b shows that each petal is of bottlelike morphology, namely, ZnO nanobottles, and the heights of the nanobottles are 200−500 nm. The inset in Figure 6b clearly shows several so-called ZnO nanobottles.

Nanocombs and Nanowheels of ZnO Nanoarrows. If the weight ratio of In/In_2S_3 was further increased to 2:1, comblike ZnO nanostructures of periodic ZnO nanowire arrays were produced (Figure 7a). It reveals that arrow-shaped branches with uniform diameters and lengths are evenly distributed at one side of the stem. The diameters of the nanoarrows are about 30 nm with caps 100 nm in diameter. The length of a single ZnO nanoarrow is about 2 μm. Though the comblike ZnO nanostructures have already been reported by several groups, the presently formed comblike ZnO nanostructutures are composed of one or two sets of ZnO nanoarrows grown on the stem instead of ZnO nanowires with uniform diameters along the length.[29] When the substrate temperature is carefully adjusted, the growth of one-sided or two-sided nanocombs can be easily controlled. This result is similar to the report of Wang and co-workers.[29] Figure 7b is the SEM image of two-sided ZnO nanocombs, which are also composed of arrowlike ZnO branches grown perpendicular to the stems.

In addition to the significant portion of ZnO nanocombs observed in Figures 7a and 7b, the most striking feature of the sample is the formation of wheellike structures by rolling up ZnO nanocombs, which has never been found before. These novel nanowheels have been indicated with arrows in Figures 7a and 7b. Figure 7c shows the high-magnification SEM image of a single ZnO nanowheel. The nanowheel is folded from a one-sided nanocomb. The composed branched wirelike ZnO crystallites are actually ZnO nanoarrows with lengths of 1 μm, and the diameters of the trunks are 50 nm. Recently, Wang[32,33] and co-workers reported the formation of perfect ZnO nanorings. In their studies, the growth of the nanoring structures can be

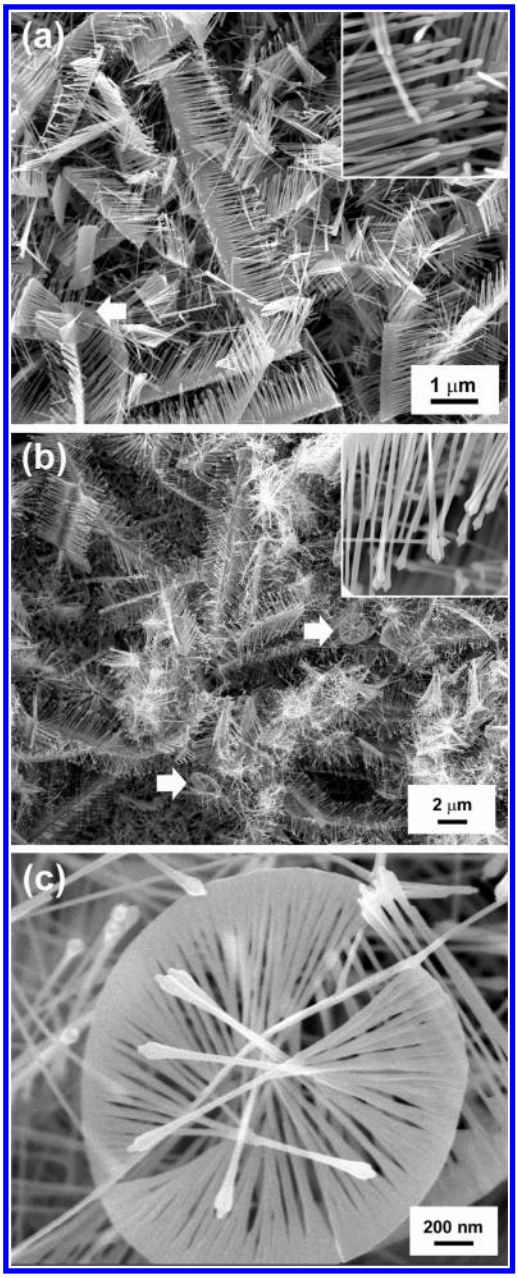

Figure 7. SEM image of nanocombs and nanowheels from ZnO nanoarrows when the weight ratio of In/In_2S_3 is 2:1.

understood from the polar surfaces of the ZnO nanobelts. The polar nanobelt, which is the building block of the nanorings, has polar charges on its top and bottom surfaces. If the surface changes are uncompensated during growth, then the nanobelt may tend to fold itself as its length gets longer to minimize the area of the polar surface. So it results in neutralization of the local polar charges and a reduced surface area, thus forming a loop with an overlapped end. The long-range electrostatic interaction is likely to be the initial driving force for folding the nanobelt to form the first loop for the subsequent growth. In our experiments, it must be mentioned that all of the ZnO nanowheels are folded from only one-sided nanocombs. Therefore, it is suggested that the formation of ZnO nanowheels may be also driven by long-range electrostatic interactions. During the formation of ZnO nanowheels, the one-sided nanocomb structure first is formed, and then the alignment of the ZnO nanoarrow arrays on only one side of the comblike structures destroys the balance of the electrostatic interaction. As a result, the nanocomb tends to fold itself as its length gets longer to

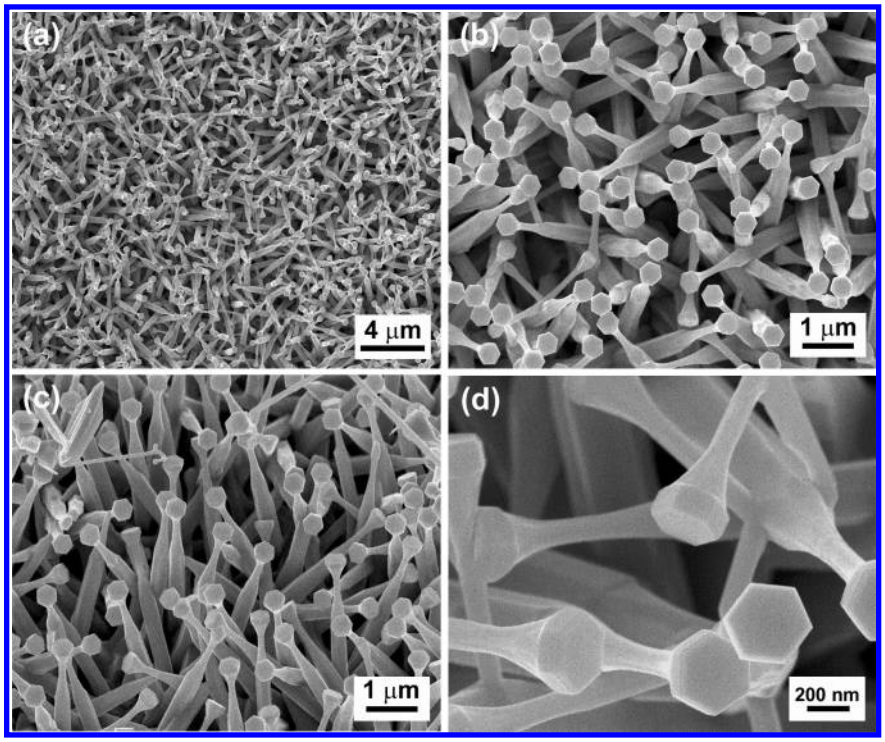

Figure 8. ZnO nanonail arrays produced from Zn powder and In powder.

minimize the area of the polar surface, and finally the nanocomb turns into the nanowheel nanostructure. Further studies are necessary to understand the growth mechanism in more detail and to control the experimental parameters to improve the yield of ZnO nanowheels.

ZnO Nanonails and Nanofans. If the weight ratio of In/In_2S_3 was increased to 3:1 or pure In powder was used instead of the mixture of In and In_2S_3, ZnO nanonail arrays were obtained (Figures 8a and 8b). Each ZnO nanonail is 2−4 μm in length with a perfect hexagonal-shaped cap about 300 nm in diameter. A side-view SEM image shown in Figure 8c indicates that these ZnO nanonails grow quasi-aligned on the substrate. Figure 8d is the high-magnification image of several ZnO nanonails, which clearly shows that the ZnO nanonails obtained from the present method are composed of perfect hexagonal prism caps and prism shafts connected with smaller diameter necks. Through the use of this process, the formation of ZnO nanonails does not require low pressures or high temperatures, which would be of benefit to produce high-quality ZnO nanonails to study their properties and potential applications.

We also tried to synthesize ZnO Nanostructures using Zn and In_2S_3 powder as the source materials. Figure 9a shows the SEM image of the ZnO products obtained from Zn and In_2S_3 powder. Novel fanlike crystals are obtained on a large scale. Figure 9b is the image of a single ZnO nanofan. It shows that the ZnO nanofan is composed of a set of ZnO nanonail arrays evenly distributed at the main stem. The ZnO nanonail arrays can be clearly seen in Figure 9c. We think that the formation of these novel ZnO nanofans is also driven by the same long-range electrostatic interactions as the formation of ZnO nanowheels. According to our experimental results, it was suggested that by adjusting the molar ratio of In and In_2S_3 powders, we can control novel self-organized hierarchical ZnO nanoarchitectures with their construction units, including ZnO nanocones, nanobowling pins, nanobottles, nanoarrows, and nanonails.

Growth Mechanism. The formation of complicated hierarchical ZnO nanoarchitectures indicates that complicated reactions may be occurring in the present experiments. Though it is still not completely clear what exactly happened between In, In_2S_3, and Zn during the growth, undoubtedly In and In_2S_3 and their weight ratio are of critical importance for these complicated structures as in the above results. During the evaporation, In and In_2S_3 are first evaporated to generate the corresponding gases at high temperature, and then they are transferred by Ar gas to the low-temperature region. During the transfer period, In_2S_3 gases decompose to generate In and S gases slowly.[34] In the low-temperature region where the Si substrate is located, the slowly generated In gas, which originates from In powder and the decomposition of In_2S_3 powder, condenses together with the generated Zn gases in the low-temperature region and forms the liquid droplets of the Zn−In−O−S eutectic phase. After supersaturation of Zn and O elements, ZnO nanoarchitectures begin to form. The oxygen may originate from the residual oxygen in the quartz tube and the alumina boat at high growth temperatures. The concentration of the slowly released In gas, which originates from In powder, the decomposition of In_2S_3, and the formation of the Zn−In−O−S eutectic phase are the critical factors to the growth of hierarchical ZnO nanoarchitectures. Though the Zn−In−O−S eutectic phase may form during the growth process, we could not detect the existence of indium or sulfur through XRD and EDX analyses. The exact growth mechanism undoubtedly needs further studies.

PL Properties. As a wide-band-gap semiconductor, ZnO is of interest in low-voltage and short-wavelength (green or green-blue) electrooptical devices. Figure 10 shows the room-temperature PL spectra from the obtained ZnO nanoarchitectures. All of the products show similar PL properties though they have great differences in morphologies. The room-temperature PL spectra show greatly enhanced green emissions centered at about 520 nm, which is in agreement with previous reports.[35,36] Besides the green emission, ZnO nanonails obtained from Zn powder and In powder also show a weak UV emission located at about 380 nm. The UV emission can be assigned to the band gap of ZnO, which comes from the recombination of free excitons as noted in previous reports.[37,38] To further study the PL properties of the present ZnO nanoarchitectures, we fit

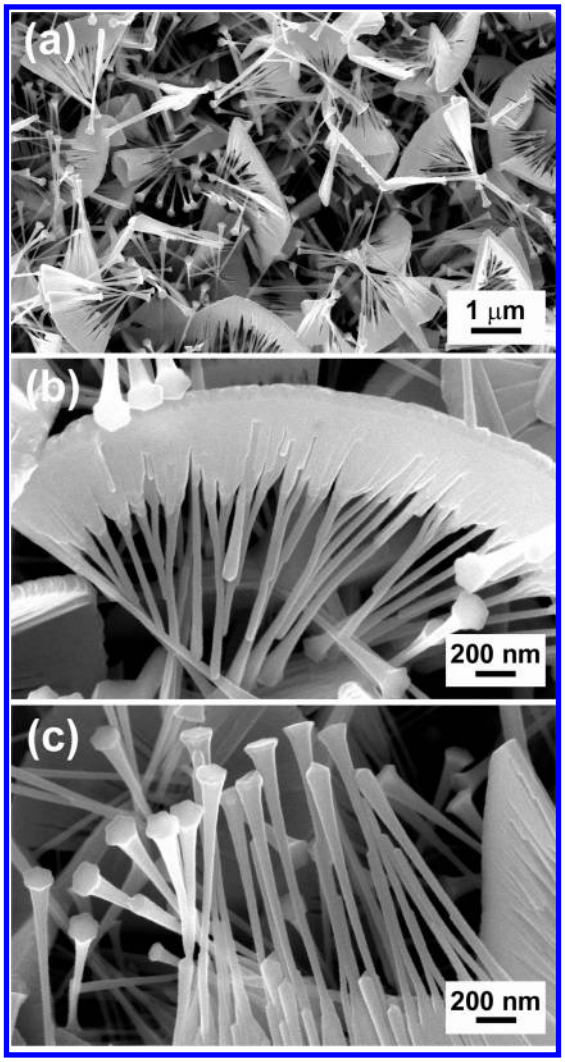

Figure 9. ZnO nanofans obtained from Zn powder and In_2S_3 powder.

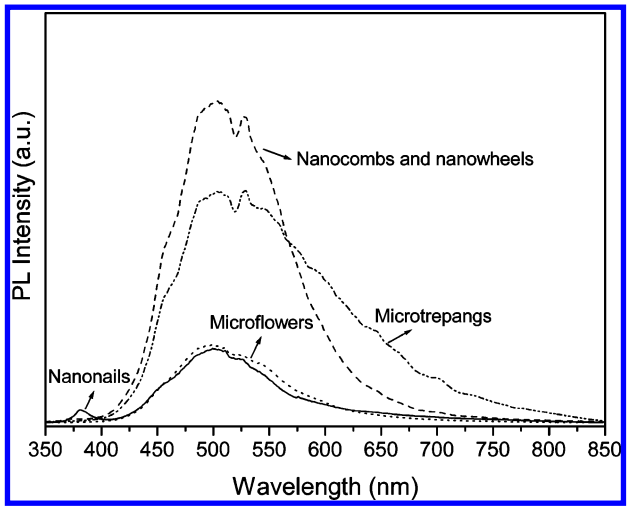

Figure 10. Photoluminescence spectra recorded at room temperature from the obtained hierarchical ZnO nanoarchitecutes.

the green emission at 520 nm using Gaussian simulations because the simulations can provide further information about the origin of the emission in this region. The green emission centered at around 520 nm can be fitted as a sum of three Gaussians, one in the blue and the other two in the green and yellow regions. According to previous reports, the blue emission peak is caused by the intrinsic defects (O and Zn vacancies or interstitials in ZnO nanowires).[39,40] The origin of the green emission peak is somewhat controversial though there have been many reports on this emission. The commonly accepted explanation is that the green emission is due to a transition between a singly ionized oxygen vacancy and a photoexcited hole.[41] And other mechanisms, such as copper impurities, donor−acceptor complexes, Zn vacancy, antisite oxygen, etc., were also proposed.[41−43] In comparison to the green emission, the yellow part of the emission is less controversial, and we think that it arises from the single negatively charged oxygen ion (O_i^-) inside of the ZnO crystal structure as reported previously.[44] The enhancement of the green emission of the presently synthesized trepanglike ZnO nanostructures is of great interest for typical applications of ZnO phosphors, such as field emissive display technology.

4. Conclusion

The controlled growth of novel hierarchical ZnO nanoarchitectures including microtrepangs of ZnO nanocones, microbelts of ZnO nanobowling-pin arrays, nanoflowers of ZnO nanobottles, nanocombs and nanowheels of ZnO nanoarrows, and nanofans of ZnO nanonails have been realized on Si substrates. This synthetic method does not require low pressures or high temperatures and is a very simple and controllable process. These novel hierarchical nanoarchitectures can potentially be used to fabricate nanoelectronic devices and construct nanobuilding blocks for further nanosystems.

References and Notes

(1) Xia, Y. N.; Yang, P. D.; Sun, Y. G.; Wu, Y. Y.; Mayers, B.; Gates, B.; Yin, Y. D.; Kim, F.; Yan, H. Q. *Adv. Mater.* **2003**, *15*, 353.
(2) Rao, C. N. R.; Deepak, F. L.; Gundiah, G.; Govindaraj, A. *Prog. Solid State Chem.* **2003**, *31*, 5.
(3) Rao, C. N. R.; Gundiah, G.; Deepak, F. L.; Govindaraj, A.; Cheetham, A. K. *J. Mater. Chem.* **2004**, *14*, 440.
(4) Zhang, B. P.; Binh, N. T.; Segawa, Y.; Wakatsuki, K.; Usami, N. *Appl. Phys. Lett.* **2003**, *83*, 1635.
(5) Dong, L. F.; Jiao, J.; Tuggle, D. W.; Petty, J. M.; Elliff, S. A.; Coulter, M. *Appl. Phys. Lett.* **2003**, *82*, 1096.
(6) Pan, Z. W.; Dai, Z. R.; Wang, Z. L. *Science* **2001**, *291*, 1947.
(7) Dai, Z. R.; Pan, Z. W.; Wang, Z. L. *Adv. Funct. Mater.* **2003**, *13*, 9.
(8) Huang, M. H.; Mao, S.; Feick, H.; Yan, H.; Wu, Y.; Kind, H.; Weber, E.; Ruso, R.; Yang, P. *Science* **2001**, *292*, 1897.
(9) Zhao, Q. X.; Willander, M.; Morjan, R. R.; Hu, Q. H.; Campbell, E. E. B. *Appl. Phys. Lett.* **2003**, *83*, 165.
(10) Wang, Z. L. *Adv. Mater.* **2003**, *15*, 432.
(11) Gao, P. X.; Wang, Z. L. *J. Phys. Chem. B* **2004**, *108*, 7534.
(12) Park, J. H.; Choi, H. J.; Sohn, S. H.; Park, J. H. *J. Mater. Chem.* **2004**, *14*, 35.
(13) Li, J. Y.; Chen, X. L.; Li, H.; He, M.; Qian, Z. Y. *J. Cryst. Growth* **2001**, *233*, 5.
(14) Liu, C. H.; Zapien, J. A.; Yao, Y.; Meng, X. M.; Lee, C. S.; Fan, S. S.; Lifshitz, Y.; Lee, S. T. *Adv. Mater.* **2003**, *15*, 838.
(15) Lyu, S. C.; Zhang, Y.; Lee, C. J.; Ruh, H.; Lee, H. J. *Chem. Mater.* **2003**, *15*, 3294.
(16) (a) Lee, C. J.; Lee, T. J.; Lyu, S. C.; Zhang, Y.; Ruh, H.; Lee, H. J. *Appl. Phys. Lett.* **2002**, *81*, 3648. (b) Ham, H.; Shen, G. Z.; Cho, J. H.; Lee, T. J.; Seo, S. H.; Lee, C. J. *Chem. Phys. Lett.* **2005**, *404*, 69.
(17) Bae, S. Y.; Seo, H. W.; Choi, H. C.; Park, J.; Park, J. *J. Phys. Chem. B* **2004**, *108*, 12318.
(18) Wu, J. J.; Liu, S. C. *Adv. Mater.* **2002**, *14*, 215.
(19) Kong, Y. C.; Yu, D. P.; Zhang, B.; Fang, W.; Feng, S. Q. *Appl. Phys. Lett.* **2001**, *78*, 407.
(20) Greyson, E. C.; Babayan, Y.; Odom, T. W. *Adv. Mater.* **2004**, *16*, 1348.
(21) Vayssieres, L. *Adv. Mater.* **2003**, *15*, 464.
(22) Choy, J. H.; Jang, E. S.; Won, J. H.; Chung, J. H.; Jang, D. J.; Kim, Y. W. *Adv. Mater.* **2003**, *15*, 1911.
(23) Liu, B.; Zeng, H. C. *J. Am. Chem. Soc.* **2003**, *125*, 4430.
(24) Geng, C. Y.; Jiang, Y.; Yao, Y.; Meng, X. M.; Zapien, J. A.; Lee, C. S.; Lifshitz, Y.; Lee, S. T. *Adv. Funct. Mater.* **2004**, *14*, 589.
(25) Park, W. I.; Yi, G. C.; Kim, M. Y.; Pennycook, S. J. *Adv. Mater.* **2002**, *14*, 1841.

(26) Park, W. I.; Kim, D. H.; Jung, S. W.; Yi, G. C. *Appl. Phys. Lett.* **2002**, *80*, 4232.
(27) Yan, H. Q.; He, R. R.; Pham, J.; Yang, P. D. *Adv. Mater*. **2003**, *15*, 402.
(28) Gao, P. X.; Wang, Z. L. *Appl. Phys. Lett.* **2004**, *84*, 2883.
(29) Wang, Z. L.; Kong, X. Y.; Zuo, J. M. *Phys. Rev. Lett.* **2003**, *91*, 185502.
(30) (a) Shen, G. Z.; Cho, J. H.; Lee, C. J. *Chem. Phys. Lett.* **2005**, *401*, 414. (b) Lao, J. Y.; Wen, J. G.; Ren, Z. F. *Nano Lett.* **2002**, *2*, 1287.
(31) Lao, J. Y.; Huang, J. Y.; Wang, D. Z.; Ren, Z. F. *Nano Lett.* **2003**, *3*, 235.
(32) Kong, X. Y.; Ding, Y.; Yang, R.; Wang, Z. L. *Science* **2004**, *303*, 1348.
(33) Kong, X. Y.; Wang, Z. L. *Nano Lett.* **2003**, *3*, 1625.
(34) *Handbook of Inorganic Compounds Synthesis*; The Chemical Society of Japan, Ed.; Chemical Industry Press: Beijing, China, 1986.
(35) Hu, J. Q.; Bando, Y.; Zhan, J. H.; Li, Y. B.; Sekiguchi, T. *Appl. Phys. Lett.* **2003**, *83*, 4414.
(36) Zhang, J.; Yu, W.; Zhang, L. *Phys. Lett. A* **2002**, *299*, 276.
(37) Wong, E. M.; Searson, P. C. *Appl. Phys. Lett.* **1999**, *74*, 2939.
(38) Stikant, V.; Clarker, D. R. *J. Appl. Phys.* **1998**, *83*, 5447.
(39) Li, D.; Leung, Y. H.; Djurisic, A. B.; Liu, Z. T.; Xie, M. H.; Shi, S. L.; Xu, S. J.; Chan, W. K. *Appl. Phys. Lett.* **2004**, *85*, 1601.
(40) Hu, J. Q.; Ma, X. L.; Xie, Z. Y.; Wong, N. B.; Lee, C. S.; Lee, S. T. *Chem. Phys. Lett.* **2001**, *344*, 97.
(41) Reynolds, D. C.; Look, D. C.; Jogai, B. *J. Appl. Phys.* **2001**, *89*, 6189.
(42) Garces, N. Y.; Wang, L.; Bai, L.; Giles, N. C.; Halliburton, L. E.; Cantwell, G. *Appl. Phys. Lett.* **2002**, *81*, 622.
(43) Studenikin, S. A.; Cocivera, M. *J. Appl. Phys.* **2002**, *91*, 5060.
(44) Liu, M.; Kitai, A. H.; Mascher, P. *J. Lumin.* **1992**, *54*, 35.